ACS APPLIED MATERIALS & INTERFACES

Research Article

www.acsami.org

# Interface Strain-Induced Multiferroicity in a $SmFeO_3$ Film

Zhenxiang Cheng,*[,†] Fang Hong,[†] Yuanxu Wang,*[,‡] Kiyoshi Ozawa,[§] Hiroki Fujii,[§] Hideo Kimura,[§] Yi Du,[†] Xiaolin Wang,[†] and Shixue Dou[†]

[†]Institute for Superconducting and Electronics Materials, University of Wollongong, Innovation Campus, North Wollongong, New South Wales 2519, Australia

[‡]Institute for Computational Materials Science, School of Physics and Electronics, Henan University, Kaifeng, 475004, People's Republic of China

[§]National Institute for Materials Science, Sengen 1-2-1, Tsukuba, Japan

**ABSTRACT:** An epitaxial pseudocubic $SmFeO_3$ thin film on (100) Nb-$SrTiO_3$ was studied based on ferroelectric (FE) characterization and magnetic measurements. High-resolution transmission electron microscopy images clarify the nature of the epitaxial growth, the stress-induced structural distortion at the film/substrate interface, and the existence of two different orientation lattices. Clear grain boundaries can be seen, which could introduce an extra local distortion. Rectangular FE loops can be observed at room temperature, even by just applying a small voltage ranging from −1 to +1 V, indicative of the presence of FE polarization. Piezoelectric force microscopy images confirm the existence of FE domains and the switchable polarization. A strong ferromagnetic-like transition occurs around 185 K, which is much lower than the transition observed in the bulk sample. It is believed that the pseudocubic structure enhances FE polarization and decreases the magnetic ordering temperature, which is confirmed by the first-principles theoretical calculations. Meanwhile, the ferroelectricity in this thin film should originate from distortion and modification in the structural modules rather than from the exchange striction interaction that is found in the bulk $SmFeO_3$.

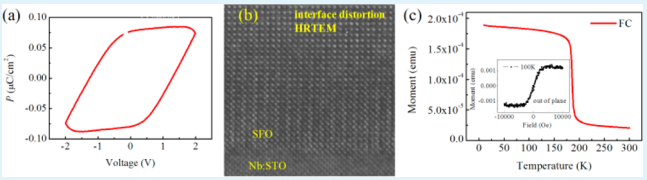


**KEYWORDS:** *strain, multiferroicity, interface*

## INTRODUCTION

The wide application of traditional data storage is attributed to the giant magnetoresistance effect.[1,2] Because of increasing demands for more computing power and data storage, a new type of unit cell with higher data density and lower power consumption is required. Ferroelectric (FE) random access memory seems to be a good choice, in which vertical polarization can be easily achieved, meaning that high density could be obtained. Meanwhile, the stability of FE domains ensures that information can be well saved for a long time. On the other hand, one special type of material in which magnetic ordering and FE ordering can coexist, the so-called multiferroic materials, also shows great potential for the next generation of data storage applications and other kinds of spintronic devices because spin freedom can be operated beyond charge freedom. Therefore, exploring new functional materials having multiferroic properties has been a highly topical research field in recent years.[3−7]

$BiFeO_3$ has shown its priority because of its room temperature multiferroic property.[8] $Bi^{3+}$ is not friendly to the environment or to human health, however, and obtaining a single phase on a large scale is still a problem, which could increase the cost of production. Furthermore, the weak magnetization at room temperature, weak magnetoelectric coupling, and large electrical coercive field strongly limit its practical application. Rare-earth manganites, such as $DyMnO_3$[9−11] and $TbMnO_3$[10](space group *Pnma*), are of great interest because electric polarization is induced by spiral magnetic ordering because of the simultaneously broken spatial inversion and time-reversal symmetries.[12] In addition, the FE property can also be found in antiferromagnetic (AFM) hexagonal $HoMnO_3$ and $YMnO_3$ (space group $P6_3cm$).[13,14] The FE property of these two materials originates from the buckling of layered $MnO_5$ polyhedral units, driven by the size effect and electrostatic interaction as well. In these manganites, the spiral magnetic ordering temperatures are very low and far away from room temperature, which restricts their application at common ambient temperatures. Most traditional FE materials, such as lead zirconate titanate (PZT) and $BaTiO_3$, are not magnetic. Therefore, finding new multiferroic materials with strong ferroelectricity and a high magnetic transition temperature seems to be the unavoidable way to achieve real applications.

Up to now, there have been few reports on FE studies of the orthoferrites, except for $DyFeO_3$ and $SmFeO_3$ (SFO).[15−17] From the point of view of symmetry, it is nearly impossible to achieve a FE phase in orthorhombic ferrite. In the case of $DyFeO_3$, the FE transition takes place below the magnetic transition temperature of the $Dy^{3+}$ lattice around 3.5 K, which can be explained by the exchange−striction interaction. As for

Received: February 5, 2014
Accepted: April 30, 2014
Published: April 30, 2014

  

SFO, a small polarization is supposed to occur because of the symmetric exchange−striction interaction among canted AFM spins,[18,19] so it shares FE origins similar to those of $DyFeO_3$[15] and $CaMn_7O_{12}$.[20−22] Strain engineering has been employed to produce low-dimensional materials such as functional thin films, and this method has introduced many unique properties that are not possessed by their corresponding bulk forms. Recently, ferroelectricity has been reported in an artificial hexagonal $YbFeO_3$ thin film on a hexagonal substrate.[23]

In this work, however, we study epitaxial pseudocubic SFO on a (001) $SrTiO_3$ (STO):Nb substrate prepared by pulsed laser deposition (PLD). Assuming that the mismatch between the two sets of lattices could introduce strain and lead to local structural distortion at the film/substrate interface, the structure and physical properties of the thin film may consequently be modified. Our characterization shows that a FE loop is present at room temperature, and piezoresponse force microscopy (PFM) images confirm the switchable FE domain structure. Meanwhile, magnetic measurement results show that SFO experiences a ferromagnetic (FM)-like (canted AFM) transition around 185 K, quite different from bulk SFO, which is indicative of the multiferroic property in this material. Transmission electron microscopy (TEM) confirms the local structural distortion induced by the strain effect and consequent symmetry change at the film/substrate interface. First-principles calculations confirm FE polarization in the pseudocubic distorted SFO film.

## EXPERIMENTAL SECTION

$SmFeO_3$ (SFO) thin films were deposited at 830 °C on (001) Nb-$SrTiO_3$ (STO) in a dynamic flowing oxygen atmosphere of 200 mTorr, using a PLD system. The SFO target was prepared by the solid-state reaction method, and X-ray diffraction (XRD; model GBC MMA, Cu K$\alpha$ radiation) shows that it is a single phase with an orthorhombic structure. A Nd:YAG laser source was used with 355 nm wavelength. During the deposition process, the laser was stabilized at 6−7 J/cm$^2$, and pulses were repeated at 10 cycles/s. The crystal structures of the films were examined by XRD at room temperature. The thickness of the films was determined by scanning electron microscopy (SEM; model JEOL JSM-6460A) and is around 450 nm. High-resolution TEM (HRTEM; model JEOL JEM-4000EX) clarified the epitaxial growth of the thin film at the interface and the existence of boundaries that separate the majority $[010]_0$ and minority $[101]_0$ lattices. The magnetic properties were measured by a superconducting quantum interference device (SQUID) magnetometer. Platinum electrodes were deposited on the film for FE measurements by magnetron sputtering with a standard shadow mask. A FE analyzer (TF2000, aixACCT) was employed to characterize the FE properties (FE hysteresis loops and fatigue). Meanwhile, PUND mode measurements were performed to reveal the real switching process. Nanoscale FE measurements of an as-grown SFO film were carried out via PFM (model MFP-3D Asylum Research). The typical scan size and rate were 500 nm and 0.1 Hz, respectively. Positive and negative direct-current bias of 5 V was applied to the tip to produce a switched domain structure, and subsequent scanning was done at 370 kHz in dual alternating-current resonance tracking (DART) PFM mode.

For first-principles calculations, an initial distorted structure was used. The redefined crystal axes of the SFO film were set as $a//[10\bar{1}]_0$, $b//[010]_0$, and $c//[101]_0$ of the orthorhombic structure of bulk SFO. The lattice parameters $a$ and $b$ of the film were set as $a = b = 7.81$ Å $= 2c$ for the STO, while the out-of-plane lattice parameter $c$ and angle $\beta$ were relaxed. During this process, other parameters, $a$ and $b$ and the angles $\alpha$ and $\gamma$, were fixed. The relaxed and distorted SFO crystal structure is $a = b = 7.81$ Å, $c = 7.44$ Å, $\alpha = 90°$, $\beta = 92.09°$, and $\gamma = 90°$. The calculations were performed using the project-augmented-wave method implemented in the Vienna ab initio simulation package.

## RESULTS AND DISCUSSION

The SFO thin film was prepared by PLD on a (001) STO:Nb single-crystal substrate. The basic structure was examined by XRD, as shown in Figure 1. The XRD pattern reveals that the

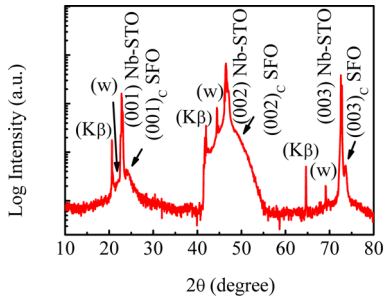


**Figure 1.** XRD pattern of a pseudocubic SFO film deposited on a (001) STO:Nb single-crystal substrate.

SFO is epitaxially grown and three satellite peaks are found near the (001), (002), and (003) STO:Nb peaks. This is similar to the case of the $LuFeO_3$ and $BiFeO_3$ films on a (001) STO substrate, which are both "cube-on-cube", grown epitaxially with a pseudocubic structure. Considering the similarity between epitaxial $BiFeO_3$[24,25] and SFO, it is reasonable to tentatively assign the SFO film to the rhombohedral or hexagonal structure. A structural study based on diffraction peak calculations shows that the three peaks of the pseudocubic structure can successfully be assigned to the (012), (024), and (217) peaks of the rhombohedral structure ($R3c$, $a_r = 5.638$ Å, and $\alpha_r = 52.64°$) or to the (102), (204), and (217) peaks of the hexagonal structure ($P6_3cm$, $a_h = b_h = 5.00$ Å, $c_h = 14.53$ Å, $\alpha = \beta = 90°$, and $\gamma = 120°$).

Compared with the sharp diffraction peaks from the substrate, the three peaks from the thin film are relatively broad, which may originate from two sets of reflections from close sets of lattice parameters. To find out how the thin film really grows, HRTEM was employed to determine the interface structure, as shown in Figure 2. The cross section of the thin film was imaged in bright-field mode, in which a clear interface between the thin film and substrate can be seen. In Figure 2, a specifically selected film/substrate interface highlighted in the dotted rectangular frame is magnified in the upper left corner.

Considering the lattice mismatch between the orthorhombic SFO and the cubic STO, stress-induced distortion should exist at the film/substrate interface. The TEM image of the film/substrate interface clearly shows the atomic rearrangement in an exactly cubic structure that is gradually relaxed to orthorhombic. In addition, two types of growth along different crystallographic directions of orthorhombic SFO were found. A structural transition boundary is clearly shown in the TEM image. According to the TEM image and the selected-area electron diffraction (SAED) pattern, the growth direction of the SFO film in relation to the substrate orientation can be determined, which is shown in Figure 2b,c. The out-of-plane directions of the SFO film on a (100) STO substrate are $\langle 101\rangle_0$ and $\langle 010\rangle_0$, respectively. Therefore, the three satellite diffraction peaks in the XRD patterns from low to high angles can be assigned to $1/2(101)_0$, $(101)_0 + (010)_0$, and $3/2(101)_0$. This also explains why the diffraction peak of the film at around $2\theta = 48°$ is broad, because it contains two sets of diffraction peaks in very close positions. The estimated lattice spacing $d_{101}$ is 3.79 Å, which is significantly reduced in comparison with the

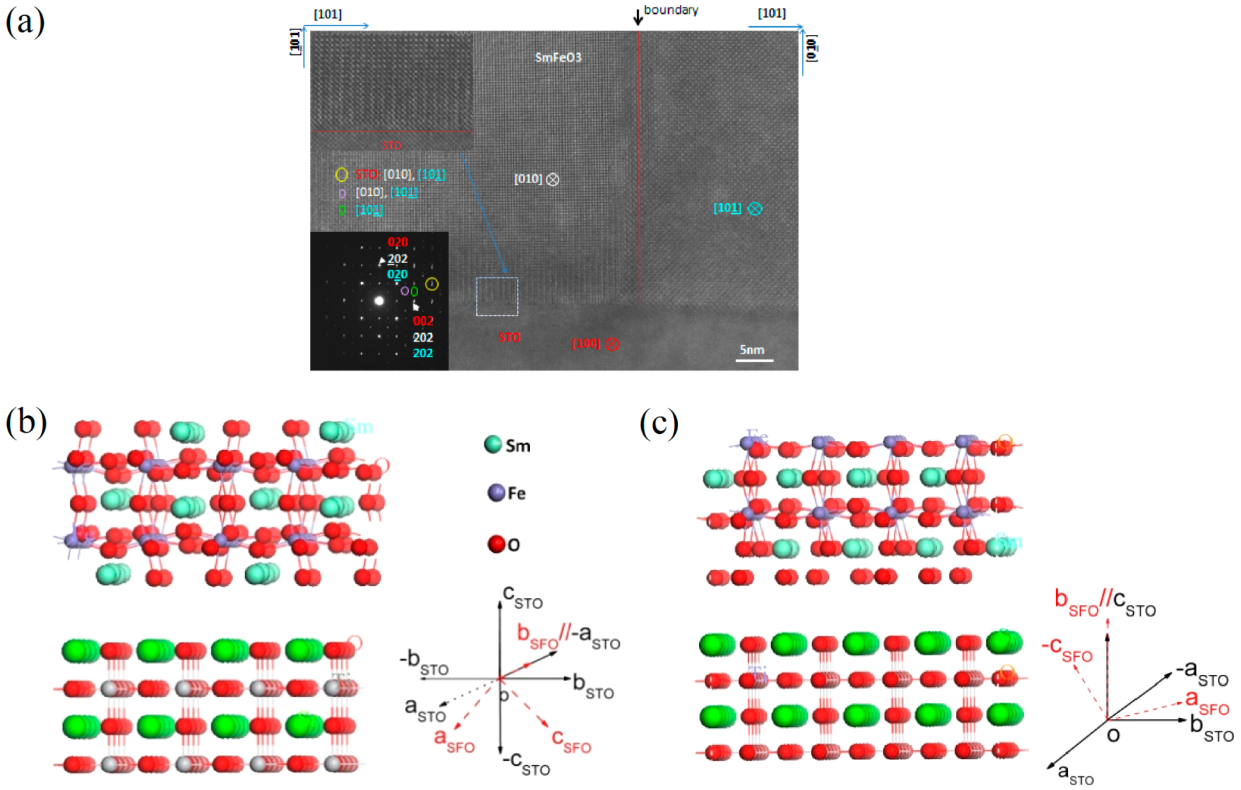


**Figure 2.** (a) Interface between the SFO thin film and the STO substrate, on which the grain boundary of $[010]_0$ and $[101]_0$ grains is also shown. The inset in the upper left corner is the HRTEM image of the film/substrate interface, magnified from the selected $[010]_0$ growth area shown in the dotted rectangular frame. The inset in the lower left corner is the SAED pattern, where the high-level diffraction spot shows a splitting, indicating the different structures existing in the film. Parts b and c contain the schematic structures of the two different growth orientations of the film, $\langle 101\rangle_0$ and $\langle 010\rangle_0$, respectively. In this figure, the crystallographic directions of an orthorhombic structure of a bulk phase were used in order to show the correspondence between the film growth direction and bulk structure.

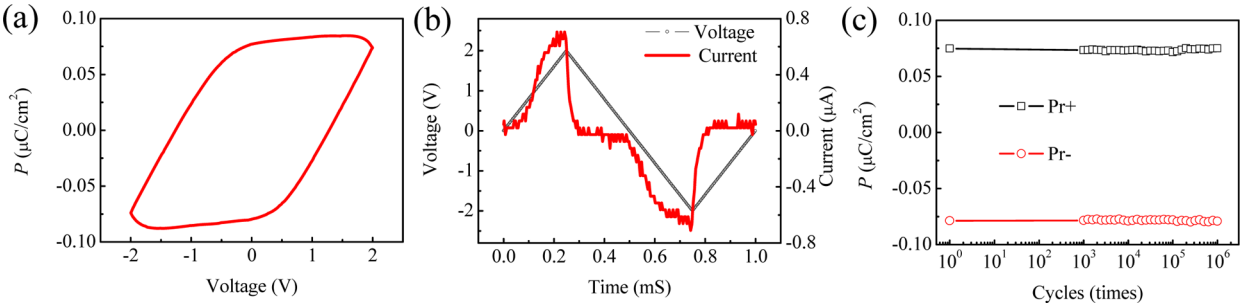


**Figure 3.** (a) Electrical hysteresis loop of the SFO film on STO:Nb at room temperature. (b) Time dependence of the applied voltage and corresponding current. (c) Fatigue test results after $10^6$ cycles (10 data points every decade).

bulk value of 3.89 Å. Such a reduction is caused by elongation of the $b$ axis due to the fact that $b_{SFO}$ = 7.706 Å, which is less than $2a$ = 7.806 Å of STO. This estimation is based on the part of the film with $\langle 101\rangle_0$ growth, although the part of the film with $\langle 010\rangle_0$ growth may not exhibit a significant change in the lattice parameter because the in-plane $d_{101}$ lattice spacing matches well with $d_{100}$ of the STO substrate. Therefore, the so-called epitaxial growth actually includes two sets of growth directions. The part of the film with $\langle 101\rangle_0$ growth shows significant distortion with reduced $a$ and $c$ and elongated $b$. Such a structural distortion will cause orbital and spin reconstruction and result in novel properties.

The existence of the two sets of growth will introduce grain boundaries with disorder or rearrangement of the atoms, which can be clearly observed in the TEM image in Figure 2. The boundary between the [010] and [101] lattices should also introduce extra stress and local structural distortion in this system. The epitaxial growth of the film will gradually relax, and therefore the structural distortion will be released when the film grows thicker. The boundaries between lattices with two different orientations always exist, however, which is beyond the scale of the stress on the interface.

Electric hysteresis loops of SFO films on STO:Nb were collected at room temperature. When the applied voltage exceeds 1.2 V (electric field ~22 kV/cm), a quasi-rectangular loop can be observed, as shown in Figure 3a, indicating a strong FE property. A higher applied voltage will increase the leakage current, and a relatively round FE loop will be present (not shown). The time dependence of the applied voltage and consequent current are given in Figure 3b, in which an obvious

switching current can be seen, which is quite different from the typical resistor or capacitor behavior. The small difference in the current behavior between opposite voltages is probably due to the electrode effect (Au and Nb-STO). To check the fatigue properties, P−E loops were measured $10^6$ times, and the remanent polarizations are presented in Figure 3c. The remanent polarization is about 0.08 $\mu C/cm^2$. There was no significant change in the remanent polarization after the fatigue test, indicating the good stability of this FE material.

Considering the leakage effect, which can also contribute to P−E loops, we used the positive-up negative-down (PUND) method to confirm the real polarization. The PUND method uses an up−up−down−down wave to exclude the leakage effect. The standard PUND wave form is presented in Figure 4.

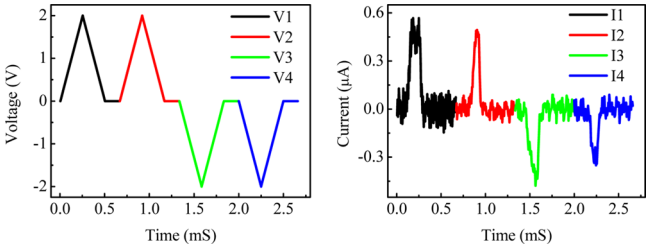


**Figure 4.** Time dependence (left) of the applied voltage (ranging from −2 to +2 V) and consequent current (right) measured in the PUND mode.

At the beginning, the system uses a negative writing pulse to polarize the film. After that, a positive pulse V1 is applied to the film, and a current will be produced as a result of leakage and domain flipping. Then, another positive pulse V2 is applied, and a current will be produced but only as a result of leakage. Therefore, the integrity of the current difference produced between up−up or down−down processes is in accordance with 3 times the remanent polarization, $2P_r$. This also applies to the down−down process. A V3 pulse will switch the FE domains to the opposite direction, and V4 just measures the leakage current contribution. In Figure 4, a clear difference in the current between I1 and I2 or between I3 and I4 can be observed (because the pure leakage current peak is lower and narrower than that when it is combined with the switching current), indicating that polarization in the P−E loop is real. The real current contribution from FE switching is reduced to half, however, meaning that the remanent polarization is about 0.04 $\mu C/cm^2$. This value is very close to that found in orthorhombic $HoMnO_3$,[26,27] in which $Mn^{3+}$ spins are in E-type AFM ordering. To some extent, considering the different magnetic states involved in the orthorhombic $HoMnO_3$ and the orthorhombic SFO, this similarity suggests that the mechanism in the orthorhombic bulk SFO may not apply to the SFO thin film.

The PFM image presented in Figure 5 shows the presence of FE domains, which are mainly dominated by two types with opposite vectors. This means that the domain walls in this film

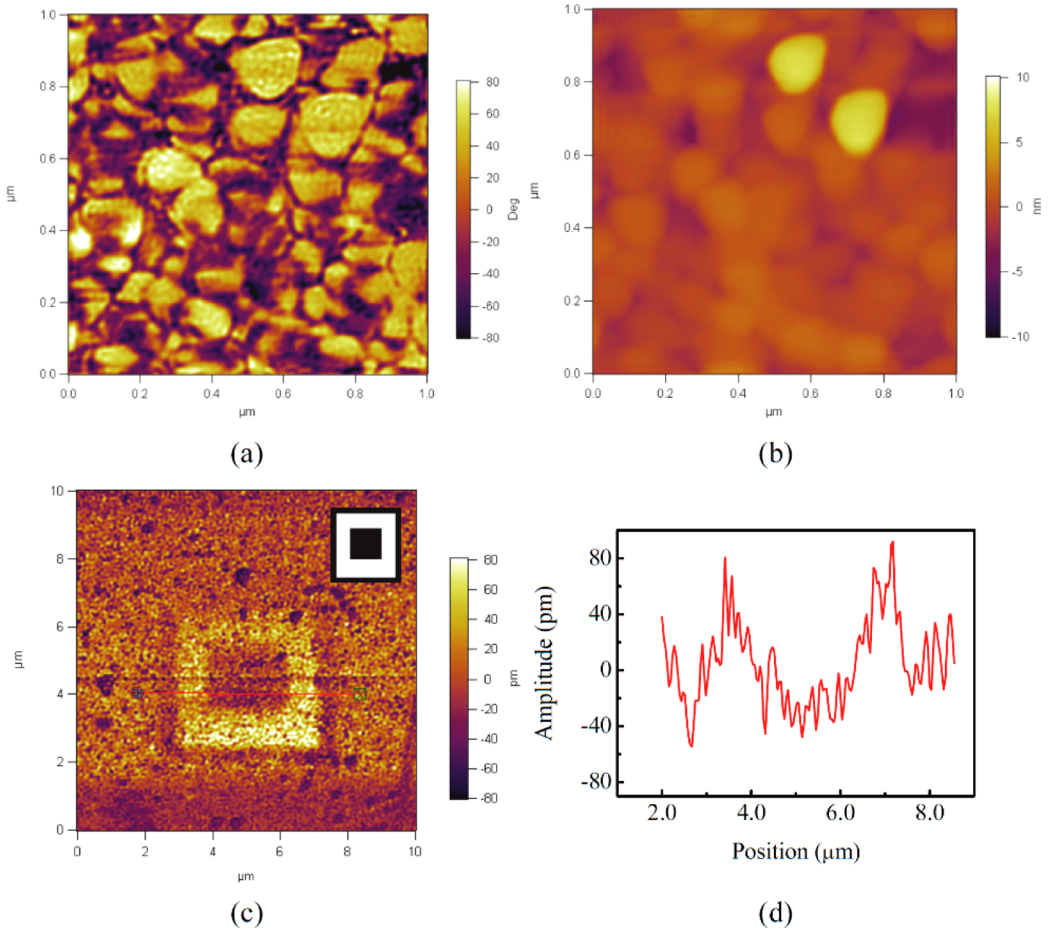


**Figure 5.** Nanoscale FE domain structure characterized by PFM: (a) phase image; (b) morphology. (c) PFM lithography pattern. Inset: preset pattern. (d) Amplitude distribution along the red line across the lithography pattern in part c.


dx.doi.org/10.1021/am500762c | ACS Appl. Mater. Interfaces 2014, 6, 7356−7362

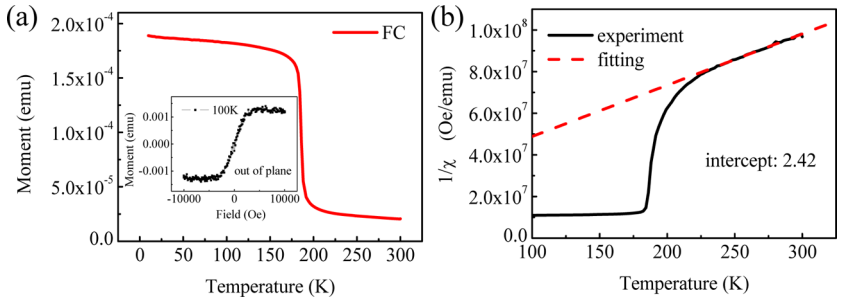


**Figure 6.** (a) Temperature dependence of a magnetic moment from 10 to 300 K and a magnetic hysteresis loop measured at 100 K (inset). (b) AFM interaction of a $Fe^{3+}$ sublattice confirmed by Curie–Weiss law fitting with a temperature range from 100 to 300 K.

are mostly 180° domain walls. Meanwhile, information on the surface morphology was also obtained, and the results show an average roughness of about 1.8 nm, indicative of a good quality film. Upon comparison of the morphology with the phase pattern, it is not difficult to see that there is more than one domain in some single grains. The average domain size is around 0.1 $\mu$m, much smaller than the domain size in the $BiFeO_3$ film.[28] One important characteristic of the ferroelectricity is that the FE domains can be controlled and reversed by an external electric field, the so-called "write". To do it, we carried out PFM lithography on the SFO film. A square-in-square pattern is obtained, as shown in Figure 5c, in which the inset is the preset pattern. The amplitude distribution along the red line across the pattern is presented in Figure 5d. It is clear that these two cubic boxes show opposite amplitude values, suggesting that they are truly two types of domains with opposite polarization directions.

To investigate the magnetic properties of this "pseudocubic" SFO film, we carried out measurements using a magnetic properties measurement system. The field-cooling temperature dependence of the magnetic moment was measured from 10 to 300 K, as shown in Figure 6a. A sharp FM-like transition can be found around 185 K. The FM behavior can be confirmed by the magnetic hysteresis loop at 100 K. Curie–Weiss law fitting gives a positive intercept, which corresponds to a negative Curie–Weiss temperature, indicating an AFM interaction starting below 240 K,[29,30] as can been seen in Figure 6b. Hence, the FM-like behavior should originate from a canted AFM ordering. This is quite different from what happens in bulk SFO, in which a spin-reorientation transition, from a canted AFM ordering to a collinear AFM ordering, takes place around 433 K. Such a big change may be attributed to $Fe^{3+}$ spin frustration, which weakens the interaction between $Fe^{3+}$ ions compared with that in the orthorhombic lattice. The stress-induced distortion on the interface and boundaries should be responsible for the significant change in the magnetic properties. This result indicates that the ferroelectricity in the SFO at room temperature may not arise from the magnetic exchange striction interaction but from structural distortion.

Bulk SFO has been reported to show spin-driven FE polarization at room temperature based on experimental measurements; however, the theoretical calculations deny such a possibility. Therefore, the multiferroic property in SFO is still controversial. Our SFO thin film, however, shows strong structural distortion at both the film/substrate interface and grain boundaries. Such structural distortion will cause reconstruction of the crystal lattice and rearrangement of the spin, and thus electrical polarization, driven by both displacement of the ions and spin. When a distorted structure of SFO was adopted at the film/substrate interface, the different magnetic states were calculated based on first-principles calculations in the framework of density functional theory (DFT), and the results are presented in Table 1. The energies

**Table 1. Calculated Total Energies of the Distorted SFO System with Different Magnetic Structures**[a]

| energy | G-type AFM | A-type AFM | C-type AFM | FM | PM | $\Delta P$ [100] ($\mu C/cm^2$) |
|---|---|---|---|---|---|---|
| $U = 0$[b] | 0 | 1.09 | 0.739 | 3.599 | 5.045 | 15.32 |
| $U = 2$[b] | 0 | 1.66 | 0.723 | 5.372 | 12.274 | 15.31 |

[a]The Hubbard $U$ values of 0 and 2 were considered in the calculation and compared. The FE polarization was calculated for G-type AFM. [b]Total energy (relative to the G-type AFM state in electronvolts/formula unit).

of those magnetic states were compared with G-type AFM ordering of iron for both Hubbard $U$ = 0 and 2, which shows that G-type AFM is the most stable state in comparison to A-type AFM, C-type AFM, FM, and paramagnetic (PM) states. The polarization is calculated as ~15.3 $\mu C/cm^2$ for both $U$ values. The value of $U$ does not show any significant effect on the magnetic state and polarization. Although the calculated polarization value is much larger than the measured value, this result indicates that the observed polarization might be caused by structural distortion at the film/substrate interface. The discrepancy might be caused by relaxation of the distorted SFO film structure to a bulk one in a relatively thick film, which has been confirmed in HRTEM images. In addition, G-type AFM easily forms a canted magnetic structure[31,32] and causes the appearance of net moment and spin-driven polarization induced by the exchange striction interaction. Although we cannot distinguish the two contributions to the polarization, i.e., ionic-displacement-driven polarization and spin-driven polarization, studying the possibility for the existence of large magnetoelectric coupling will be the aim of the next step in our research program.

Finally, we compare the calculated electron density isosurface with the value of 0.45 for undistorted and distorted SFO systems obtained from DFT calculations, which is shown in Figure 7. The electron density contour is known to be an informative tool to distingush different bonding interactions in solids. It is obversious that, in the distorted system, the electron density between oxygen and iron is strong enough to form a three-dimensional network, indicating a strong asymmetric covalent bonding interaction, while in the undistorted sytstem, the electron density between oxygen and iron is weak. For both


dx.doi.org/10.1021/am500762c | ACS Appl. Mater. Interfaces 2014, 6, 7356–7362

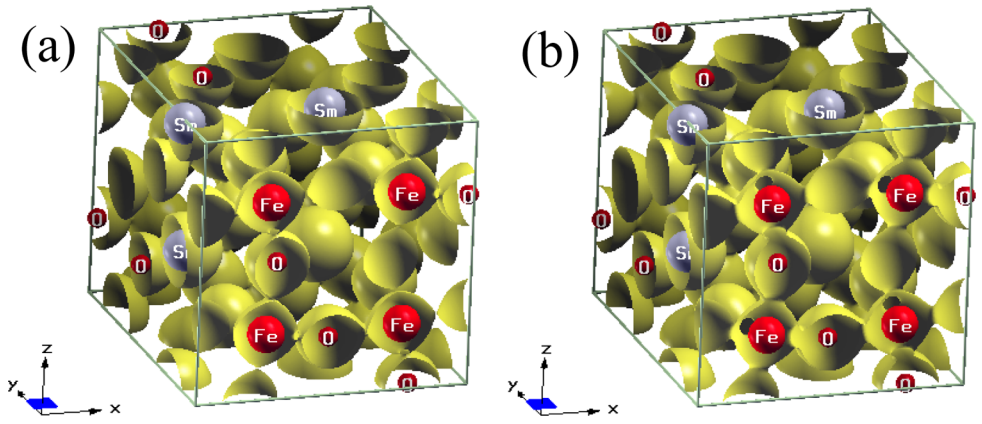


**Figure 7.** Calculated electron density isosurface with a value of 0.45 for undistorted (a) and distorted (b) SFO systems.

distorted and undistorted SFO, it is hard to see any bonding between samarium and oxygen ions. Therefore, the observed and calculated polarization has nothing obvious to do with the bonding between oxygen and samarium. In typical FE materials, like $BaTiO_3$, the asymmetric covalent bonding between Ti 3d and O 2p orbitals is the driving force for the structure distortion and thus for the appearance of the dipole.[33] However, in a strained SFO film, structural distortion is a result of the substrate clamping effect, which works as a driving force for formation of the dipole in the materials, and Fe 3d and O 2p orbital hybridization is a result of structural distortion. Therefore, the strong asymmetric covalent bonding is related to the observed polarization in the distorted SFO thin film but not a reason for the appearance of polarization.

## CONCLUSIONS

In summary, the structure and FE and magnetic properties were studied in an epitaxial pseudocubic SFO on a STO:Nb substrate. Clear structural distortion can be identified on the $[010]_0$-grown film/substrate interface, as well as boundaries of $[010]_0$ and a small fraction of $[101]_0$ grains. A strong FM-like transition is observed around 185 K, which is likely to be due to canted AFM ordering. The PFM images clarify the existence of ferroelectricity and the switchable domain structure. There is also a saturating hysteresis loop in the FE measurements, and the loops are very stable, even after $10^6$ cycles. The PUND method was used to determine the intrinsic FE polarization, and the remanent polarization is about 0.04 $\mu C/cm^2$, which is comparable to that in orthorhombic $HoMnO_3$. The structural distortion in this system is probably responsible for the significant change in the magnetic properties and the small polarization as well. The theoretical calculations of the highly distorted SFO structure have theoretically confirmed the existence of the ferroelectic polarization and net magnetic moment in the thin-film form of SFO.

## AUTHOR INFORMATION

### Corresponding Authors

*E-mail: cheng@uow.edu.au.
*E-mail: wangyx@henu.edu.cn.

### Notes

The authors declare no competing financial interest.

## ACKNOWLEDGMENTS

Z.C. thanks the Australian Research Council for support through a Future Fellowship (FT 0990287). We thank Dr. Tania Silver for carefully polishing the draft.

## REFERENCES

(1) Moritomo, Y.; Asamitsu, A.; Kuwahara, H.; Tokura, Y. Giant Magnetoresistance of Manganese Oxides with a Layered Perovskite Structure. *Nature* **1996**, *380*, 141−144.
(2) Salamon, M. B.; Jaime, M. The Physics of Manganites: Structure and Transport. *Rev. Mod. Phys.* **2001**, *73*, 583−628.
(3) Catalan, G.; Scott, J. F. Physics and Applications of Bismuth Ferrite. *Adv. Mater.* **2009**, *21*, 2463−2485.
(4) Vaz, C. A. F.; Hoffman, J.; Anh, C. H.; Ramesh, R. Magnetoelectric Coupling Effects in Multiferroic Complex Oxide Composite Structures. *Adv. Mater.* **2010**, *22*, 2900−2918.
(5) Jain, P.; Ramachandran, V.; Clark, R. J.; Zhou, H. D.; Toby, B. H.; Dalal, N. S.; Kroto, H. W.; Cheetham, A. K. Multiferroic Behavior Associated with an Order−Disorder Hydrogen Bonding Transition in Metal−Organic Frameworks (MOFs) with the Perovskite $ABX_3$ Architecture. *J. Am. Chem. Soc.* **2009**, *131*, 13625−13627.
(6) Cui, H.; Wang, Z.; Takahashi, K.; Okano, Y.; Kobayashi, H.; Kobayashi, A. Ferroelectric Porous Molecular Crystal, $[Mn_3(HCOO)_6](C_2H_5OH)$, Exhibiting Ferrimagnetic Transition. *J. Am. Chem. Soc.* **2006**, *128*, 15074−15075.
(7) Kim, S. W.; Chang, H. Y.; Halasyamani, P. S. Selective Pure-Phase Synthesis of the Multiferroic $BaMF_4$ (M = Mg, Mn, Co, Ni, and Zn) Family. *J. Am. Chem. Soc.* **2010**, *132*, 17684−17685.
(8) Smolenskiĭ, G. A.; Chupis, I. E. Ferroelectromagnets Soviet. *Phys.-Usp.* **1982**, *25*, 475−493.
(9) Zhang, N.; Wang, K. F.; Luo, S. J.; Wei, T.; Dong, X. W.; Li, S. Z.; Wan, J. G.; Liu, J. M. Effect of B-site Al-doping on electric polarization in $DyMnO_3$. *Appl. Phys. Lett.* **2010**, *96*, 252902−252904.
(10) Kimura, T.; Lawes, G.; Goto, T.; Tokura, Y.; Ramirez, A. P. Magnetoelectric Phase Diagrams of Orthorhombic $RMnO_3$ (R = Gd, Tb, and Dy). *Phys. Rev. B* **2005**, *71*, 224425−224429.
(11) Kimura, T.; Ishihara, S.; Shintani, H.; Arima, T.; Takahashi, K. T.; Ishizaka, K.; Tokura, Y. Distorted Perovskite with $e^1_g$ Configuration as a Frustrated Spin System. *Phys. Rev. B* **2003**, *68*, 060403−060407.
(12) Mostovoy, M. Ferroelectricity in Spiral Magnets. *Phys. Rev. Lett.* **2006**, *96*, 067601−067604.
(13) Lueken, H. A Magnetoelectric Effect in $YMnO_3$ and $HoMnO_3$. *Angew. Chem., Int. Ed.* **2008**, *47*, 8562−8564.
(14) Matsumoto, T.; Ishikawa, R.; Tohei, T.; Kimura, H.; Yao, Q.; Zhao, H.; Wang, X.; Chen, D.; Cheng, Z.; Shibata, N.; Ikuhara, Y. Multivariate Statistical Characterization of Charged and Uncharged Domain Walls in Multiferroic Hexagonal $YMnO_3$ Single Crystal Visualized by a Spherical Aberration-Corrected STEM. *Nano Lett.* **2013**, *13*, 4594−4601.

(15) Tokunaga, Y.; Iguchi, S.; Arima, T.; Tokura, Y. Magnetic-Field-Induced Ferroelectric State in $DyFeO_3$. *Phys. Rev. Lett.* **2008**, *101*, 097205.
(16) Du, Y.; Cheng, Z. X.; Wang, X. L.; Dou, S. X. Lanthanum-Doped Multiferroic $DyFeO_3$: Structural and Magnetic Properties. *J. Appl. Phys.* **2010**, *107*, 09D908.
(17) Lee, J.-H.; Jeong, Y. K.; Park, J. H.; Oak, M.-A.; Jang, H. M.; Son, J. Y.; Scott, J. F. Spin-Canting-Induced Improper Ferroelectricity and Spontaneous Magnetization Reversal in $SmFeO_3$. *Phys. Rev. Lett.* **2011**, *107*, 117201−117204.
(18) Johnson, R. D.; Terada, N.; Radaelli, P. G. Comment on "Spin-Canting-Induced Improper Ferroelectricity and Spontaneous Magnetization Reversal in $SmFeO_3$". *Phys. Rev. Lett.* **2012**, *108*, 219701−219701.
(19) Reply: Lee, J.-H.; Jeong, Y. K.; Park, J. H.; Oak, M.-A.; Jang, H. M.; Son, J. Y.; Scott, J. F.; Lee. *Phys. Rev. Lett.* **2012**, *108*, 219702 (published May 21).
(20) Zhang, G.; Dong, S.; Yan, Z.; Guo, Y.; Zhang, Q.; Yunoki, S.; Dagotto, E.; Liu, J. M. Multiferroic properties of $CaMn_7O_{12}$. *Phys. Rev. B* **2011**, *84*, 174413−174417.
(21) Johnson, R. D.; Chapon, L. C.; Khalyavin, D. D.; Manuel, P.; Radaelli, P. G.; Martin, C. Giant Improper Ferroelectricity in the Ferroaxial Magnet $CaMn_7O_{12}$. *Phys. Rev. Lett.* **2012**, *108*, 067201−067205.
(22) Lu, X. Z.; Whangbo, M. H.; Dong, S.; Gong, X. G.; Xiang, H. J. Giant Ferroelectric Polarization of $CaMn_7O_{12}$ Induced by a Combined Effect of Dzyaloshinskii-Moriya Interaction and Exchange Striction. *Phys. Rev. Lett.* **2012**, *108*, 187204−187207.
(23) Jeong, Y. K.; Lee, J.-H.; Ahn, S.-J.; Song, S.-W.; Jang, H. M.; Choi, H.; Scott, J. F. Structurally Tailored Hexagonal Ferroelectricity and Multiferroism in Epitaxial $YbFeO_3$ Thin-Film Heterostructures. *J. Am. Chem. Soc.* **2012**, *134*, 1450−1453.
(24) Singh, M. K.; Jang, H. M.; Ryu, S.; Jo, M.-H. Polarized Raman Scattering of Multiferroic $BiFeO_3$ Epitaxial Films with Rhombohedral *R3c* Symmetry. *Appl. Phys. Lett.* **2006**, *88*, 042907−042903.
(25) Ihlefeld, J. F.; Kumar, A.; Gopalan, V.; Schlom, D. G.; Chen, Y. B.; Pan, X. Q.; Heeg, T.; Schubert, J.; Ke, X.; Schiffer, P.; Orenstein, J.; Martin, L. W.; Chu, Y. H.; Ramesh, R. Adsorption-controlled Molecular-beam Epitaxial Growth of $BiFeO_3$. *Appl. Phys. Lett.* **2007**, *91*, 071922−071923.
(26) Feng, S. M.; Chai, Y. S.; Zhu, J. L.; Manivannan, N.; Oh, Y. S.; Wang, L. J.; Yang, Y. S.; Jin, C. Q.; Kim, K. H. Determination of the Intrinsic Ferroelectric Polarization in Orthorhombic $HoMnO_3$. *New J. Phys.* **2010**, *12*, 073006−073011.
(27) Chai, Y. S.; Oh, Y. S.; Wang, L. J.; Manivannan, N.; Feng, S. M.; Yang, Y. S.; Yan, L. Q.; Jin, C. Q.; Kim, K. H. Intrinsic Ferroelectric Polarization of Orthorhombic Manganites with E-type Spin Order. *Phys. Rev. B* **2012**, *85*, 184406−184410.
(28) Zhao, T.; Scholl, A.; Zavaliche, F.; Lee, K.; Barry, M.; Doran, A.; Cruz, M. P.; Chu, Y. H.; Ederer, C.; Spaldin, N. A.; Das, R. R.; Kim, D. M.; Baek, S. H.; Eom, C. B.; Ramesh, R. Electrical Control of Antiferromagnetic Domains in Multiferroic $BiFeO_3$ Films at Room Temperature. *Nat. Mater.* **2006**, *5*, 823−829.
(29) Hong, F.; Cheng, Z.; Zhao, H.; Kimura, H.; Wang, X. Continuously Tunable Magnetic Phase Transitions in the $DyMn_{1-x}Fe_xO_3$ system. *Appl. Phys. Lett.* **2011**, *99*, 092502−092505.
(30) Hong, F.; Cheng, Z.; Wang, X. Strong 4f Electron Interaction and Magnetic Ordering Modification in $Nd_{1-x}Er_xMnO_3$ (0 less than or equal to *x* less than or equal to 0.5). *Appl. Phys. Lett.* **2011**, *99*, 192503−192503.
(31) Meiklejohn, W. H.; Bean, C. P. New Magnetic Anisotropy. *Phys. Rev.* **1956**, *102*, 1413−1414.
(32) Meiklejohn, W. H.; Bean, C. P. New Magnetic Anisotropy. *Phys. Rev.* **1957**, *105*, 904−913.
(33) Cohen, R. E. Origin of Ferroelectricity in Perovskite Oxides. *Nature* **1992**, *358*, 136−138.